THE OFFICIAL MAGAZINE OF THE OCEANOGRAPHY SOCIETY

Oceanography

CITATION

de Jong, M.F., M. Oltmanns, J. Karstensen, and L. de Steur. 2018. Deep convection in the Irminger Sea observed with a dense mooring array. *Oceanography* 31(1):50–59, https://doi.org/10.5670/oceanog.2018.109.

DOI

https://doi.org/10.5670/oceanog.2018.109

Deep Convection in the Irminger Sea Observed with a Dense Mooring Array

By M. Femke de Jong, Marilena Oltmanns, Johannes Karstensen, and Laura de Steur

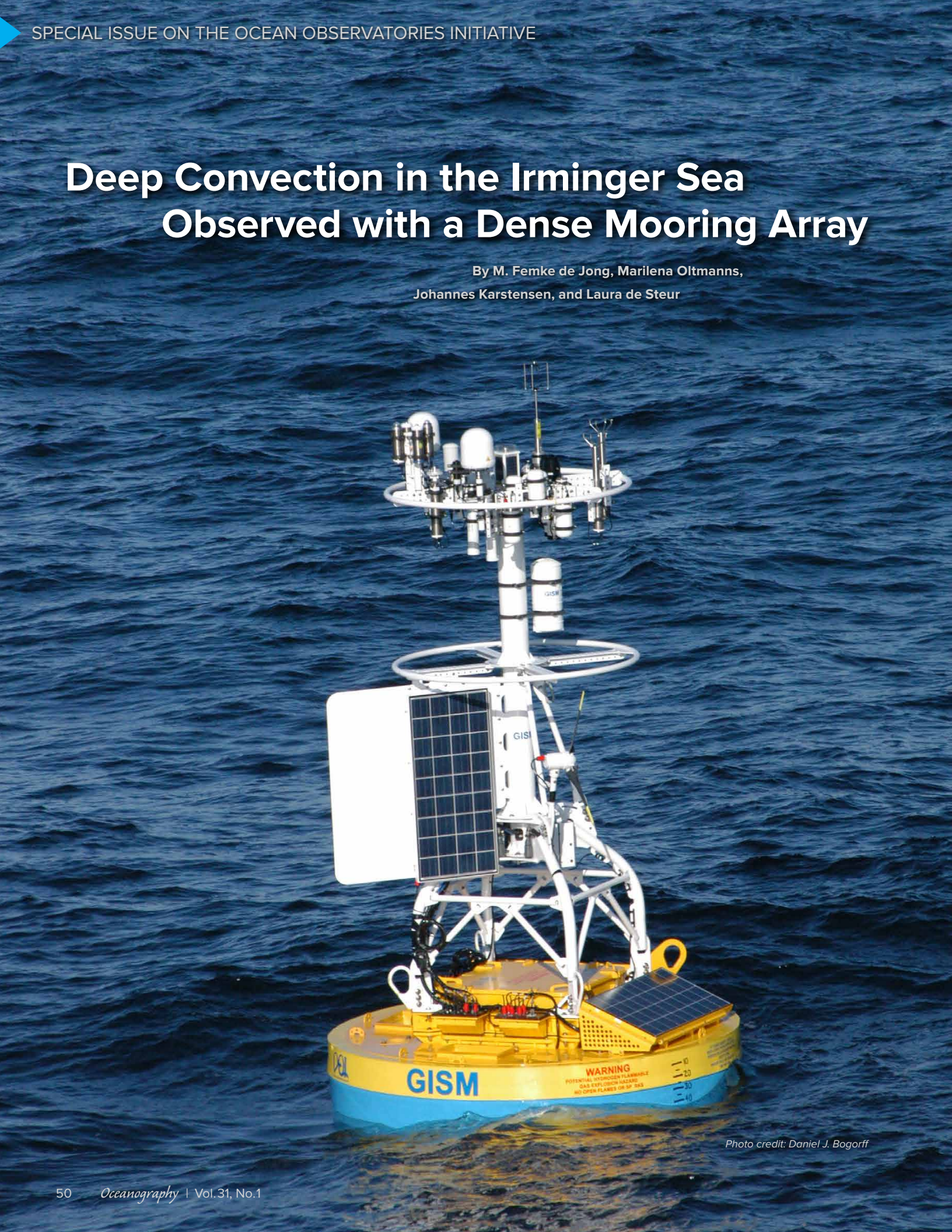

Photo credit: Daniel J. Bogorff

> Only high-resolution spatial and temporal observations can provide sufficient detail for learning more about the impact of eddies on restratification, and the relationship of restratification to convective mixing.

ABSTRACT. Deep convection is a key process in the Atlantic Meridional Overturning Circulation, but because it acts at small scales, it remains poorly resolved by climate models. The occurrence of deep convection depends on weak initial stratification and strong surface buoyancy forcing, conditions that are satisfied in only a few ocean basins. In 2014, one of the Ocean Observatories Initiative (OOI) global arrays was installed close to the Central Irminger Sea (CIS) and the Long-term Ocean Circulation Observations (LOCO) moorings in the central Irminger Sea. These programs' six moorings are located in the center of an area of deep convection and are distributed within a 50 km radius, thus offering detailed insight into spatial differences during the strong convection events that occurred during the winters of 2014/2015 and 2015/2016. Deep mixed layers, down to approximately 1,600 m, formed during both winters. The properties of the convectively renewed water mass at each mooring converge to a common temperature and salinity before restratification sets in at the end of winter. The largest differences in onset (or timing) of convection and restratification are seen between the northernmost and southernmost moorings. High-resolution atmospheric reanalysis data show there is higher atmospheric forcing at the northernmost mooring due to a more favorable position with respect to the Greenland tip jet. Nevertheless, earlier onset, and more continuous cooling and deepening of mixed layers, occurs at the southernmost mooring, while convection at the northern mooring is frequently interrupted by warm events. We propose that these warm events are associated with eddies and filaments originating from the Irminger Current off the coast of Greenland and that convection further south benefits from cold inflow from the southwest.

INTRODUCTION

Ventilation of the ocean's deep layers is a process that combines intense water mass transformation in so-called "deep-water formation areas" and the subsequent export of the waters. Only a limited number of deepwater formation areas have been identified globally, including the Weddell and Ross Seas in the Southern Ocean, the Gulf of Lyon in the Mediterranean, the Greenland Sea, and the Labrador and Irminger Seas in the North Atlantic. All of these regions are characterized by a marginally stable water column at mid-depth that underlies a seasonally stratified layer above, and strong, although intermittent, surface buoyancy losses. Heat loss is an important contributor to buoyancy loss in all areas. The haline buoyancy flux, which depends on net precipitation and, in some areas, ice melting and freezing (including brine release), is of varying importance.

The deep convection process is traditionally separated into three stages (Marshall and Schott, 1999, and references therein). The "preconditioning" stage is set by a large-scale (order of 100 km) cyclonic circulation and weak interior ocean stratification. Intense surface buoyancy flux initiates the second, "violent mixing," stage, which generates localized, intense convective plumes that have similar horizontal and vertical dimensions (order of 1–2 km). As mixing progresses, these cells organize into a larger-scale convective patch (diameter order 100 km) that is characterized by relatively homogenous properties. The third stage, "restratification," sets in when surface buoyancy flux ceases, and the density front between the convective patch and the stratified environment becomes unstable and breaks down into eddies (on the order of the Rossby deformation radius or roughly 10 km at subpolar latitudes). The net effect of these eddies is a lateral exchange that, together with recurring surface buoyancy gain, reestablishes the upper layer stratification and contributes to the export of water out of the mixed patch.

The processes active during the three stages of deep convection have been directly observed with mixed success and never in a complete sequence that covers all stages and all scales (see Schott and Marshall for a review of the experiment before 1999). In winter, field programs

have made direct observations of convective cells, including early ones (Lazier, 1973; Killworth, 1979). These high-temporal-resolution shipboard observations were generally limited to one location and the duration of a typical field program (a few weeks). Recent intense field programs, executed in the western Mediterranean Sea using ship-based and autonomous observing platforms (glider, moorings), were the first to provide further details about scales and processes for the Mediterranean deep convection across a whole seasonal cycle (Bosse et al., 2016; Houpert et al., 2016; Testor et al., 2017).

In the Irminger and Labrador Seas, which are both part of the North Atlantic Subpolar Gyre, intermittent deep convection contributes to the renewal process, creating the source waters that ultimately supply the upper North Atlantic Deep Water. The first evidence that deep convection occurs in the Irminger Sea was from ship-based observations dating to the beginning of the last century (Nansen, 1912; Sverdrup et al., 1942; Pickart et al., 2003; Våge et al., 2008; de Jong et al., 2012). Post-winter hydrographic sections, executed from the 1970s to 2000s, showed the extent of homogenous water masses in the Irminger Sea. These observations suggested deep convection had occurred during the preceding winter. In order to survey the winter conditions, two observing sites were established in the region at the beginning of the 2000s (Figure 1; Long-term Ocean Circulation Observations [LOCO], Central Irminger Sea [CIS]) with year-round observation through moored sensors and regular ship visits. The CIS site was established in September 2002 by GEOMAR (Kiel, Germany), and the LOCO site was installed one year later in September 2003; the latter has since been maintained by the Royal Netherlands Institute for Sea Research (de Jong et al., 2012).

The preconditioning phase of deep convection includes cyclonic circulation, doming of isopycnals, and large buoyancy fluxes. However, the location of the maximum doming of the isopycnals in the Irminger Gyre center is not necessarily aligned with the region of maximum wintertime thermal buoyancy loss. Atmospheric variability in this region is characterized by intense and intermittent wind events that can reach surface speeds well above 30 m s^{-1} and that result from the interaction of extratropical cyclones with the high topography of southern Greenland (Moore, 2003). Among these wind events are the so-called "Greenland tip jets" that are associated with enhanced westerly flow around the southern tip of Greenland (Doyle and Shapiro, 1999) at horizontal scales on the order of 200–400 km (Moore and Renfrew, 2005). Tip jets are known to drive significant air-sea heat fluxes in the Irminger Sea, and as such contribute to deep convection in this region (Pickart et al., 2003; Våge et al., 2008).

Depending on the alignment of the regions of the largest buoyancy forcing with those of weak stratification (defining the gyre center), deep convection may regionally vary. In 2013, the Ocean Observatories Initiative (OOI) formalized plans for installing one of its four global arrays in the Irminger Sea. The installation was targeted to improve process understanding of deep convection, and also contribute to the long-term monitoring (multi-annual to decadal) of convection in the region that had been initiated in the early 2000s with the LOCO and CIS moorings. In order to ensure the compatibility of the records already available from LOCO and CIS, the three sites were run simultaneously beginning in the summer of 2014, providing an opportunity to obtain very high sampling density (Figure 1).

The particularly strong and sustained cooling during the winter of 2014/2015 led to record deep mixing in the convection centers of the Labrador (Yashayaev and Loder, 2017) and Irminger Seas, a process that had never been directly observed in this region (de Jong and de Steur, 2016). We used this unique multi-mooring data

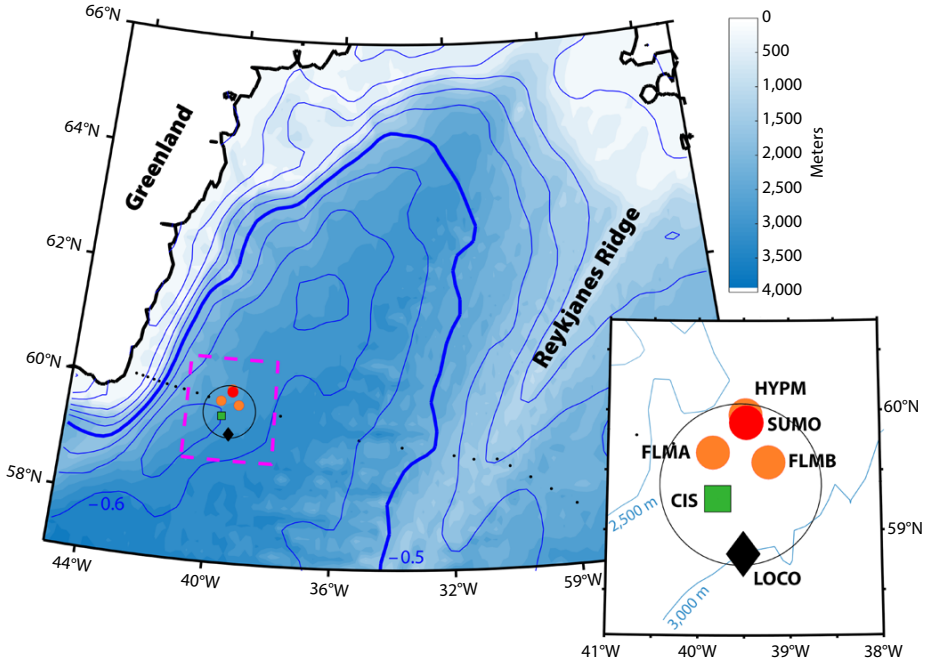

FIGURE 1. Mooring positions in the central Irminger Gyre. Contour lines of absolute dynamic topography (plotted every 0.05 m and averaged from January 1, 2014, to December 31, 2016) indicate the center of the Irminger Gyre. The map at right is close-up of the magenta dashed box in the left panel. The four Ocean Observatories Initiative (OOI) moorings are indicated by the red and orange circles, with the red circle indicating the surface mooring. The Central Irminger Sea (CIS) and Long-term Ocean Circulation Observations (LOCO) moorings are indicated by a green square and a black diamond, respectively. The six moorings are located within the 50 km radius circle drawn in black. The Overturning in the Subpolar North Atlantic Program (OSNAP) moorings in the Irminger Sea (not part of this study) are indicated by the small black dots.

set collected from 2014 to 2016 to take a detailed look into the onset, spatial evolution, and duration of convection over the winters of 2014/2015 and 2015/2016.

DATA

The OOI Irminger Sea array consists of four individual moorings. Its location was chosen to be close to the maximum doming of isopycnals derived from the contours of dynamic topography and to align with the AR7E World Ocean Circulation Experiment repeat section (Figure 2) as well as the Overturning in the Subpolar North Atlantic Program (OSNAP) array (Lozier et al., 2017). The OOI moorings contain a large variety of sensors that serve various disciplines, but for this study we focus on temperature, salinity, and velocity measurements only. The surface mooring, SUMO, consists of fixed oceanographic instruments that include SBE 37 MicroCAT conductivity and temperature recorders and Teledyne RDI acoustic Doppler current profilers [ADCPs]) along the cable down to 1,500 m, a buoy equipped with meteorological instrumentation, and a telemetric system for near-real-time data transfer. The profiling mooring, HYPM (59.98°N, 39.48°W), is outfitted with a McLane profiler that traverses the cable between 240 m and 2,400 m depth. Two flanking moorings, FLMA (59.77°N, 39.84°W) and FLMB (59.71°N, 39.32°W), are located 34.8 km apart and each about 28 km from the SUMO (59.93°N, 39.47°W) mooring. FLMA and FLMB contain instruments at discrete depths from 30 m to 2,700 m. Because we are focusing on the surface to intermediate layers affected by convective mixing, we use data from the instrumentation between the sea surface and 2,000 dbar. OOI data used here cover the period from September 10, 2014, to July 18, 2016. Details about the instruments between these levels can be found in Table 1.

The CIS mooring is located 28.6 km south of the OOI FLMA mooring at 59°31.83'N, 39°47.03'W. Before the OOI array installation, CIS was located close to SUMO/HYPM. The data analyzed here originate from the thirteenth deployment of the mooring from August 18, 2014, to May 30, 2016. At that time, the mooring was equipped with 15 MicroCATs (14 at various depths between 10 m and 1,500 m and one close to the seafloor; see Table 1), two single-point current meters (1,000 m and 2,953 m depth), and an upward-looking ADCP (150 m depth), as well as an oxygen optode and a fluorometer whose data are not used in this study. All given depths are nominal positions, but instantaneous depths may vary by several hundreds of meters, depending on mooring blow-down. The mooring was deployed with a subsurface head buoy located at about 40 m depth and a surface buoy connected with a 270 m long wire to the head buoy in order to allow the surface module to move with minimal tension on the whole mooring. This "slack wire" had a MicroCAT at 10 m depth and one at 25 m depth to obtain near-surface observational data. The surface telemetry buoy (MI.SAT1; Develogic) broke off on April 7, 2015, and the two instruments in the slack descended to about 300 m depth.

The LOCO mooring is located at 59°12.05'N/39°30.00'W, 37.8 km southeast of the CIS mooring and 58.7 km from the nearest OOI (FLMB) mooring. The mooring was outfitted with a McLane moored profiler to record daily temperature and salinity profiles between 150 m and 2,500 m depth. The LOCO mooring also contained two downward-looking ADCPs at 150 m and 2,500 m depth as well as a moored CTD near the bottom. Due to a technical failure, the LOCO profiler did not record profiles during the July 2015 to September 2016 deployment.

Mixed-layer depths (MLDs) were derived from the OOI HYPM and LOCO moored profiling data. These profiles have high vertical resolution, as the profilers record continuously while traveling along the cable. The temporal resolution (20-hour interval for OOI HYPM, 24-hour interval for LOCO) is limited due to the battery capacity of the profiler. The bottom of the mixed layer was identified from the potential temperature, practical salinity, and potential density profiles. These profiles were smoothed using a running-mean filter with a 25 dbar window to remove instrument noise. MLDs were subsequently determined employing threshold criteria of 0.015°C for temperature, 0.005 for salinity, and 0.0025 kg m^{-3} for potential density, and using the uppermost available measurement at a mooring as a reference. The uppermost measurement had to be shallower then 200 dbar

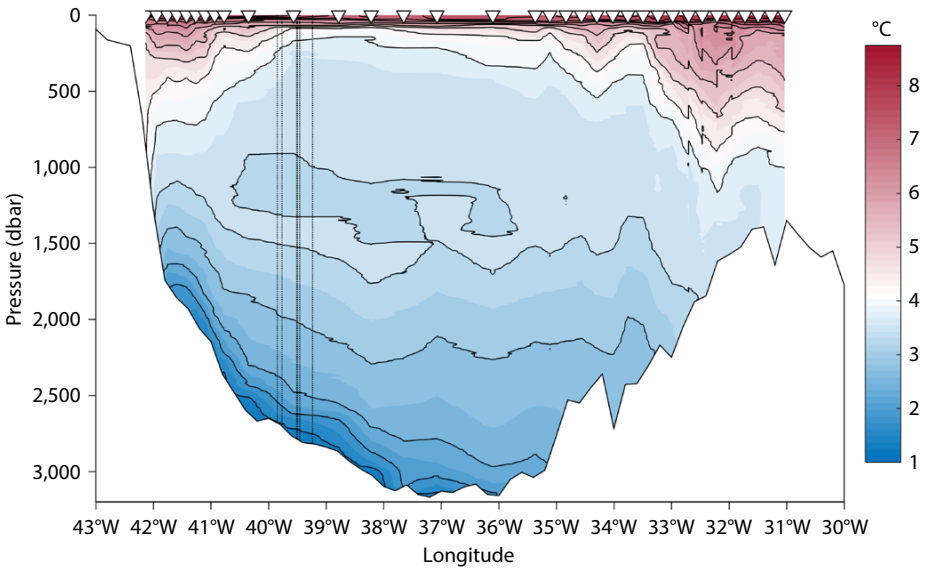

FIGURE 2. Hydrography of the Irminger Sea in summer 2015. Colors indicate potential temperature in degrees Celsius. CTD station locations are marked on the top axis by inverted white triangles. The mooring positions are projected onto the CTD line and shown as black vertical lines.

TABLE 1. Instrumentation on the six moorings used in this study. The Sea-Bird Electronics (SBE) 37, SBE 16plus, and McLane Moored Profiler (MMP) data include temperature, salinity, and pressure. The acoustic Doppler Current profilers (ADCPs) and Aquadopp Deep Water (DW) measure horizontal and vertical water velocities. The Rotating Current Meter (RCM-8) measures only horizontal velocities.

Nominal Depth (m)	OOI HYPM	OOI SUMO	OOI FLMA	OOI FLMB	CIS	LOCO
10		SBE 16plus			SBE3 7	
20		SBE 37				
30			SBE 37	SBE 37	SBE 37	
40		SBE 16plus	SBE 37	SBE 37	SBE 37	
60		SBE 37	SBE 37	SBE 37		
80		SBE 16plus				
90			SBE 37	SBE 37	SBE 37	
100		SBE 37				
130		SBE 16plus	SBE 37	SBE 37		SBE 37/ ADCP
140	SBE 37					MMP
150					ADCP	
180		SBE37	SBE 37	SBE 37		
230	MMP				SBE 37	
250		SBE37	SBE 37	SBE 37		
310					SBE 37	
350		SBE37	SBE 37	SBE 37		
390					SBE 37	
470					SBE 37	
500		SBE 37/ ADCP	SBE 37/ ADCP	SBE 37/ ADCP		
550					ADCP	
630					SBE 37	
750		SBE 37	SBE 37	SBE 37	SBE 37	
870					SBE 37	
1,000		SBE 37	SBE 37	SBE 37	Aquadopp DW	
1,250					SBE 37	
1,500		SBE 37	SBE 37	SBE 37	SBE 37	
1,700			SBE 37			
1,830				SBE 37		
2,000			SBE 37	SBE 37		
2,500						
2,550						ADCP
2,950					SBE 37/RCM-8	SBE 37

for an MLD to be registered. The resulting MLDs of all three variables had to be within 50 dbar to be accepted, after which the temperature-derived MLDs were chosen as final MLDs.

The temperature profilers from the OOI HYPM and LOCO moored profilers (limited by the uppermost instrument being at ~130 m depth) were extended toward the surface using sea surface temperature (SST) data (Group for High Resolution Sea Surface Temperature [GHRSST] at https://podaac.jpl.nasa.gov/GHRSST). GHRSST is a blended product with 0.1° resolution that was validated using the near-surface CTD data from the OOI SUMO mooring (average difference between the instrument time series at 12 m depth, and the SST is 0.085°C).

The moored CTDs on the OOI SUMO, OOI FLMA, OOI FLMB, and CIS moorings offered high temporal resolution (15 min) but limited vertical resolution (up to 250 m). For each mooring, these data were first gridded vertically onto a pressure grid with a 5 dbar interval, and then vertically interpolated. Due to the lack of a sharp transition at the bottom of the MLD in the interpolated MicroCAT data, the timing of mixing events was determined by inspecting the data for layers that have a homogeneous temperature profile and are cooling homogeneously over said layer. The chosen thresholds are $T(z)$ within 0.015°C of the temperature at 10 m depth and temperature change per 15 min interval (dT/dt) within 2.5×10^{-5} °C of the dT/dt at 10 m. The addition of the dT/dt criterion implies that active mixed layers are selected.

Mean velocities were derived for the layer between 200 m and 500 m depth using data from the upward-looking ADCP at ~500 m depth on the OOI SUMO, FLMA, and FLMB moorings and the downward-looking ADCP at ~150 m on the LOCO mooring. At the CIS mooring, we used velocity data from the single-point instrument at ~1,000 m.

The atmospheric forcing was investigated with the European Center for Medium range Weather Forecasting

(ECMWF) reanalysis ERA-Interim (ERA-I; Dee et al., 2011) and the Arctic System Reanalysis (ASR; Bromwhich et al., 2016). ASR has a higher horizontal resolution (~15 km) compared to ERA-I (~80 km), yielding an improved representation of the wind and heat flux fields (Moore et al., 2016). Because ASR data are currently available up until 2012 only, we use them to examine the spatial distribution of the heat fluxes during selected tip jet events near the moorings for the period 2000–2012 and then translate those results to the events in the winters 2014/2015 and 2015/2016 identified with ERA-I.

RESULTS

Spatial Variations in Convection

Both the winters of 2014/2015 and 2015/2016 were characterized by strong surface fluxes and deep mixed layers in the Irminger Sea (Figure 3). The 2014/2015 winter was somewhat stronger and lasted longer than the subsequent winter. The October through April mean values from the ERA-I turbulent flux were 178 W m^{-2} in 2014–2015 versus 123 W m^{-2} in 2015/2016 (Figure 3a). The daily maximum MLD was derived for the six moorings in 2014/2015 and for five moorings in 2015/2016. Despite the substantially lower heat flux in 2015/2016, mixed layers reached similar depths at the end of that winter, likely due to the extensive removal of stratification during the first winter. The local temperature variability at each mooring as well as the differences between the moorings was high during summer and quickly decreased as MLD depths reached ~250 dbar (Figure 3b,c). Progressive deepening and cooling of the mixed layer did not further reduce the variability in mixed layer properties between the moorings, indicating that a mixed patch, with homogeneous properties over the region enclosing all moorings, had formed at this time.

The velocity fields at the mooring sites,

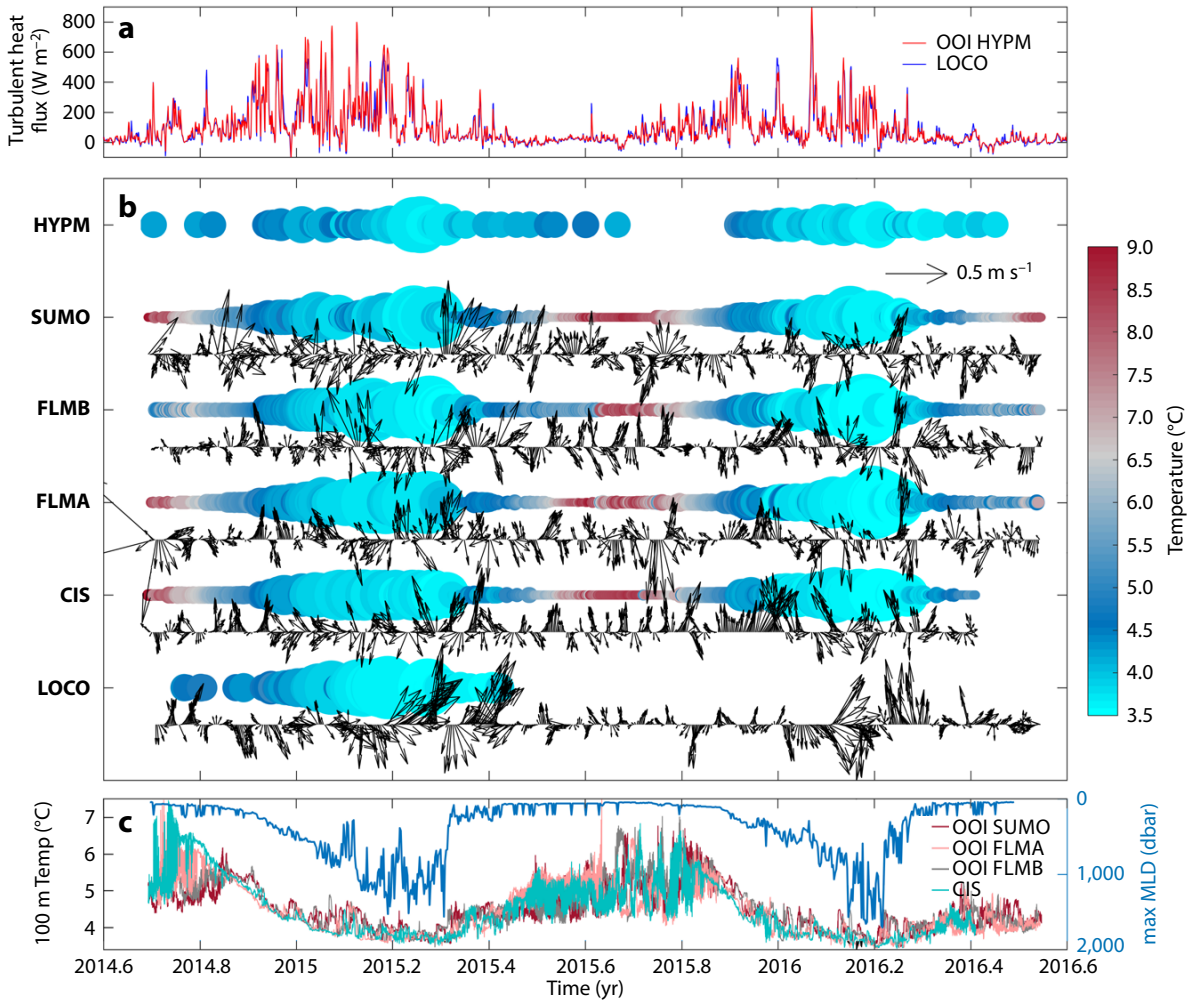

FIGURE 3. Surface fluxes and mixing during the 2014/2016 OOI deployment. (a) Time series of turbulent heat fluxes at the northernmost (red) and southernmost (blue) mooring. Data are derived from the ERA-I reanalysis. (b) Mixed layer depth, temperature, and velocity at the six moorings. Mixed layer depths are indicated by the sizes of the markers, and the mixed layer temperature is indicated with color (values are plotted daily for OOI HYPM and LOCO and thrice daily for OOI SUMO, the two flanking moorings FLMA and FLMB, and CIS). Velocity vectors are plotted every hour. Note that the velocities at the CIS mooring are obtained from a deeper depth (1,000 m rather than ~250 m). (c) Daily maximum mixed layer depth (blue) and the temperature from the four moorings with temperature measurements at 100 m depth.

displayed by the vectors in Figure 3b, showed the proximity to the center of the Irminger Gyre. Mean currents at the moorings were generally weak at the OOI moorings (between 0.6 cm s^{-1} and 1.7 cm s^{-1}) and slightly stronger toward the northeast at the CIS and LOCO moorings (3.5 cm s^{-1} and 4.2 cm s^{-1}). Despite the weak mean flow, the mesoscale field was rich (i.e., the standard deviation in velocity is 19 cm s^{-1} at the OOI moorings, 17 cm s^{-1} at LOCO, and 11 cm s^{-1} at the deeper CIS instrument). Due to the relatively large distance between the moorings compared to the Rossby radius of deformation (order 10 km), there was little coherence between the fluctuations observed at the individual moorings. The magnitude of the mesoscale variability showed a hint of the presence of a seasonal cycle, with larger velocities in winter, mostly evident at LOCO.

Although the overall picture of gradual deepening and cooling of the mixed layers through winter was similar for each mooring, there were striking latitudinal differences. At the northern OOI moorings, cooling and deepening were more intermittent, intensifying during strong surface fluxes and restratifying whenever the surface fluxes relented. At the southern moorings, CIS and LOCO, cooling and deepening were more sustained.

Of the six moorings, the OOI HYPM and the LOCO moorings were the furthest apart (85.8 km) and were the best examples of lateral contrasts. Bimonthly temperature profiles (Figure 4a) from these two moored profilers were similar at the end of summer, but clear differences appeared in January and February. Mixing and cooling progressed steadily at LOCO, while the upper 600 dbar of the OOI HYPM profiles remained stratified. Below 600 dbar, both the LOCO and HYPM moorings showed a progressive deepening of the temperature inversion, from 900 dbar in September to 1,200 dbar in February. In March and April, deep mixed layers were seen at both moorings, completely removing the temperature inversion. After April, restratification set in at both sites. A thick layer with homogeneous temperature remained at the LOCO mooring, while at the OOI HYPM, restratification appeared to be stronger, hence changing the temperature profile. Overall, the upper layer temperatures were lower and mixed layers were deeper at the LOCO mooring (Figure 4b).

Spatial Variability in Forcing and Restratification

Stratification and surface forcing determine the maximum depth of vertical mixing at a given location. The largest wintertime air-sea fluxes take place during individual intense wind events (Holdsworth and Myers, 2015). Using the high-resolution atmospheric reanalysis (ASR), we investigated the long-term spatial distribution of ocean heat loss for the area where the six moorings were deployed. The ASR data showed surprisingly large differences in heat fluxes between the mooring locations, amounting to as much as 200 W m^{-2} (Figure 5a,b). A composite of ~100 tip jet events in 2000 and 2012 showed that the differences between the mooring sites persisted, with stronger heat flux events resulting in larger differences (not shown). Generally, heat losses during tip jet events were larger at the OOI and CIS moorings and weaker at

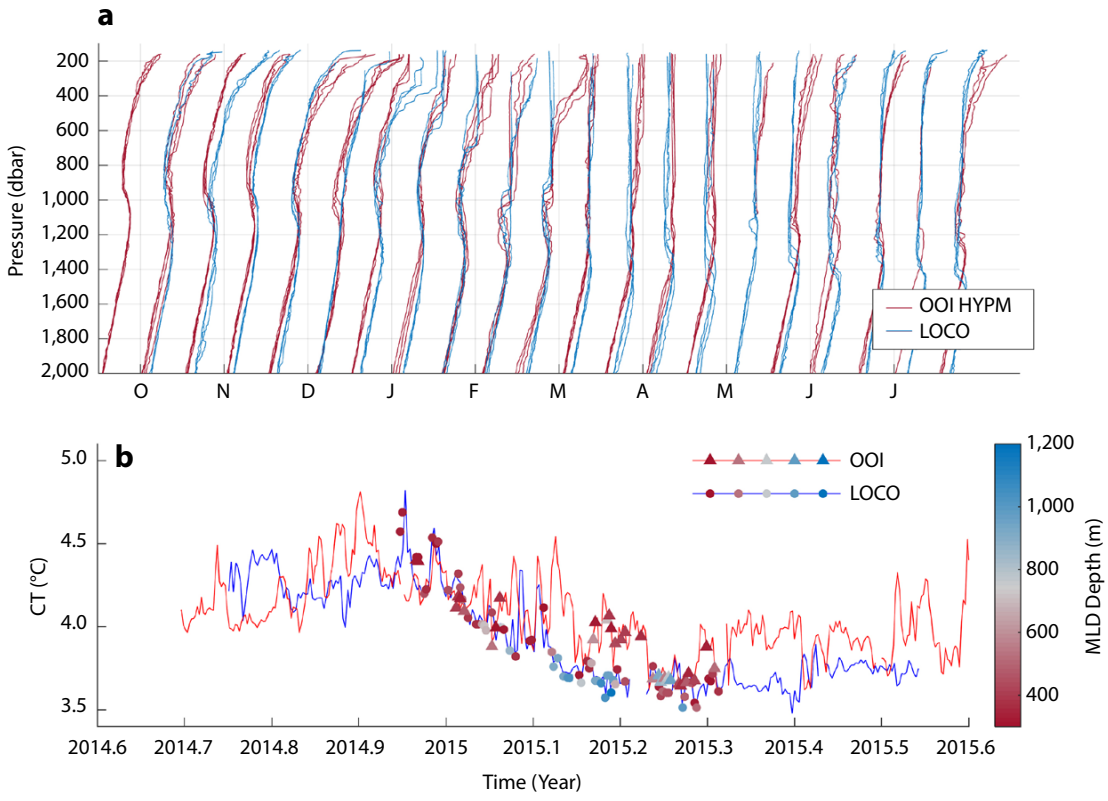

FIGURE 4. (a) Temperature profiles from the OOI (red) and LOCO (blue) moored profilers. Profiles are shown for the first and fifteenth of every month starting on September 15, 2014, for OOI and October 1, 2014, for LOCO. Each set of bimonthly temperature profiles is offset by 1°C. (b) Mean temperature over the 200 m to 500 m layer of the OOI profiles (red) and the LOCO profiles (blue). Scattered markers (triangles for OOI, circles for LOCO) indicate the temperature and the maximum depth of the mid-layer depth (MLD) in color (shown in the color scale) for MLD >200 dbar.

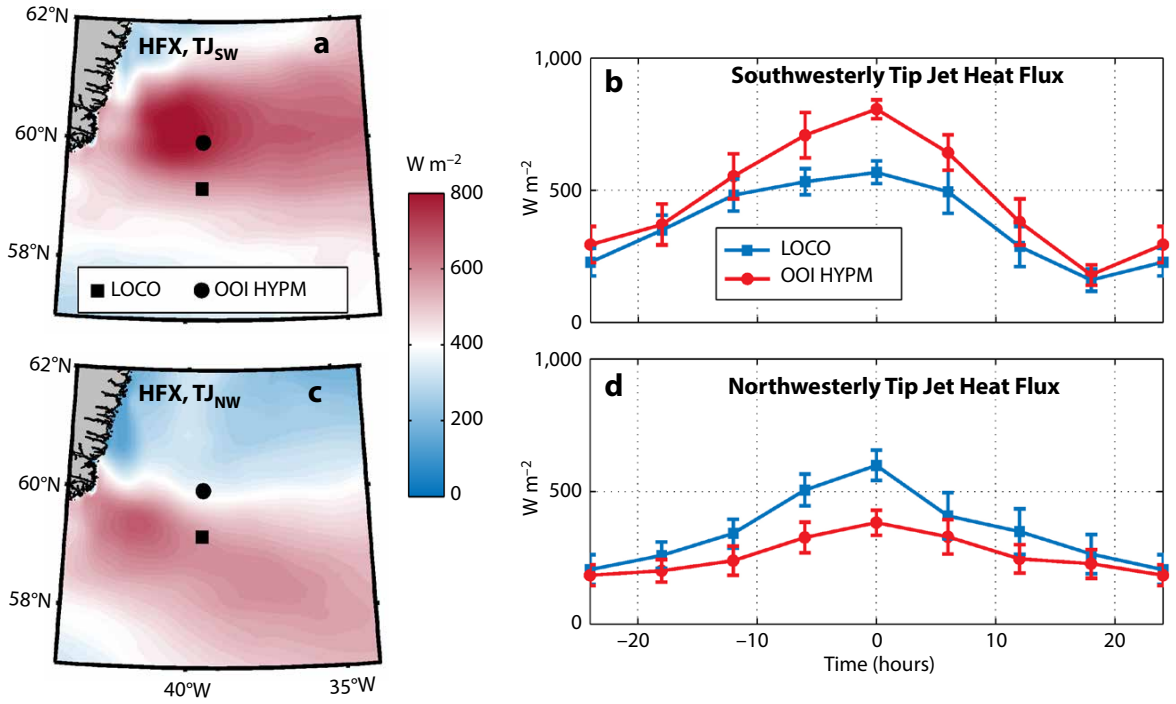

FIGURE 5. (a) Heat-flux composite based on 10 southwesterly tip jet events, obtained from the Arctic System Reanalysis. (b) Evolution of the heat fluxes associated with the southwesterly tip events shown in (a), at the location of the OOI and LOCO moorings, with the error bars indicating the standard error of the mean. (c,d) Same as (a) and (b) but for 10 northwesterly tip jet events. The south- and northwesterly tip jet events were obtained by subsampling the composite of 100 tip jets mentioned in the text.

LOCO, although at times, the heat losses at LOCO exceeded those obtained at CIS and OOI (Figure 5c,d). These wind events, associated with the largest heat losses to the south and classified as northwesterly tip jets (Moore, 2015), were generally less frequent. Both types of tip jet events were not well resolved in the much lower resolution ERA-I fields; in these smoother fields, the differences between fluxes at LOCO and OOI HYPM were reduced to 20 W m^{-2} during strong (>200 W m^{-2}) cooling events. However, the timing of strong forcing was aligned with temperature homogenization across the array and was also reflected in an increase in the variance of the vertical velocity derived from ADCP data (Figure 6a).

Despite the increased likelihood of stronger surface forcing over the OOI moorings, we observed a shallower MLD in 2014/2015 compared to LOCO, which could mean either that winter was favorable for northerly tip jets or that the OOI site was slightly less favorable for deep convection. While the initial, pre-winter

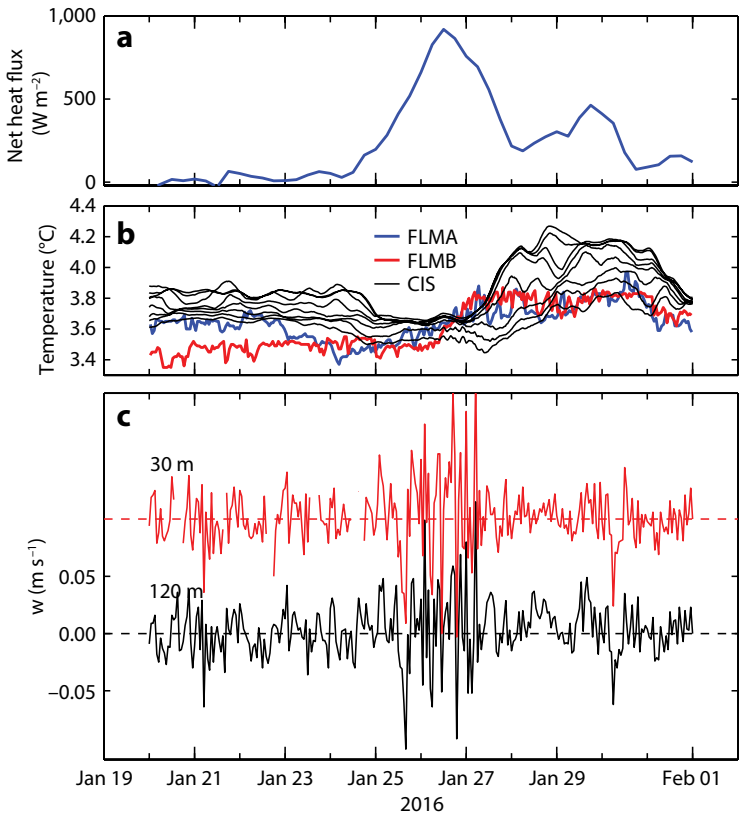

FIGURE 6. (a) ERA-I net heat flux during a tip jet event between January 26 and January 28, 2016. Accompanying (b) temperature from moorings FLMA, FLMB, and CIS, and (c) vertical velocity time series at mooring CIS from two depths of the ADCP.

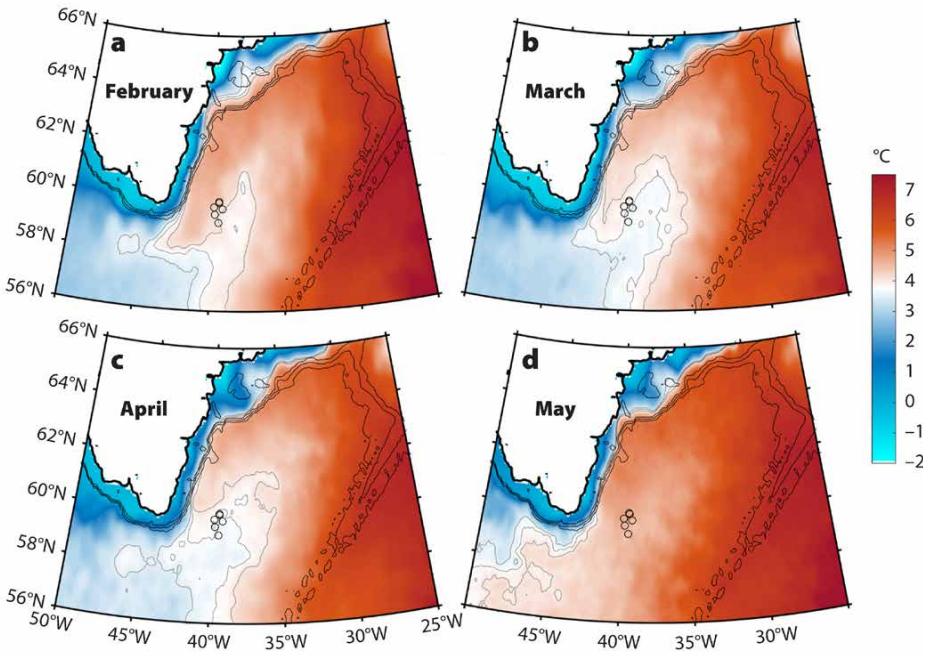

FIGURE 7. Monthly mean sea surface temperature field from the Group for High Resolution Sea Surface Temperature (GHRSST) data set for (a) February, (b) March, (c) April, and (d) May of 2015. Gray contours are drawn for the 3.5°, 3.75°, and 4°C isotherms. The mooring positions are indicated with black circles. Isobaths are drawn for 1,500 m, 1,000 m, and 500 m.

stratification was very similar throughout the area covered by the six mooring (Figure 4a), cooling at the northern OOI HYPM was frequently interrupted by short warming events (Figure 4b). These intermittent events resulted in an average heat content in the upper 1,000 m that was approximately 3% larger at OOI than at the LOCO mooring. This gradient in heat content was also reflected in the increase in SST from south to north: the mean SST over the OOI deployment period was 5.77°C at LOCO, 5.86°C at CIS, and 6.02°C at OOI HYPM. Monthly mean SST through the winter of 2015 shows that the moorings were in the low SST western part of the area (Figure 7). This colder area was east of the center of the Irminger Gyre (Figure 1), as well as east of the region with strongest surface heat fluxes in the ERA-I fields. While surface fluxes were likely dominant in regions of cooling SSTs, this suggests that cooling through advection by colder waters from the southwest may have played a role, as seen at LOCO (time periods 2015.2–2015.4 and 2016.1–2016.3 in Figure 3b) and CIS (at the end of 2015 in Figure 3b). The Irminger Current advects warmer waters along the cyclonic path around the perimeter of the basin. These warmer waters off the Greenland shelf appeared to strengthen the restratification tendency at the northern OOI mooring (Figure 4b).

DISCUSSION

The two-year data set presented here contains high-resolution data from six moorings deployed in an 86 km × 35 km area in the central Irminger Gyre. Spatial differences observed between the moorings during the winters of 2014/2015 and 2015/2016, which both showed deep (>1,500 dbar) mixed layers, revealed the subtle balance between surface forcing and intermittent restratification during winter. The close proximity of the moorings and nearly identical late summer temperature profiles suggest equal preconditioning at all sites. The more frequent occurrence of stronger tip jet events at the northern moorings has the potential to force deeper and colder mixed layers. However, the stronger surface forcing here was counteracted by frequent restratification though lateral intrusions from the warm and saline Irminger Current. Fan et al. (2013) studied the occurrence of anticyclonic warm core eddies at the CIS mooring in detail. They proposed two formation regions for the eddies: one west of the Reykjanes Ridge and the other off the East Greenland Irminger Current, near Cape Farewell. The observations presented here clearly suggest that the latter formation region was more important for restratification at the Irminger Sea OOI array.

Only high-resolution spatial and temporal observations can provide sufficient detail for learning more about the impact of eddies on restratification, and the relationship of restratification to convective mixing. These details were not caught in the much sparser Argo profile data. For comparison, there were only two Argo profiles in this area between the moorings during the period October 2014 to April 2015.

Continuation of the OOI moorings in the Irminger Sea will allow the community to study the restratification process in more detail. In addition, OOI surface measurements will allow investigation of the potential impact of freshwater that originates from the Greenland shelf on deep convection, as the influx of freshwater from the Greenland Ice Sheet and the Arctic Ocean is expected to increase with rising atmospheric and oceanic temperatures (Böning et al., 2016). Data from the OOI gliders, whose analysis was outside the scope of this paper, will yield additional insights into lateral scales of variability. Knowledge gained from an integral analysis of the full suite of OOI mooring, surface flux, and glider observations will provide more details about the full convection and restratification cycle, and will contribute significantly to improving our ability to predict deep-water formation. Integrating knowledge about physical processes with the biogeochemical data collected at the OOI array (Palevsky and Nicholson, 2018, in this issue) will lead to further insight into the controls on biological productivity and carbon cycling in the Irminger Sea.

REFERENCES

Böning, C.W., E. Behrens, A. Biastoch, K. Getzlaff, and J. Bamber. 2016. Emerging impact of Greenland meltwater on deepwater formation in the North Atlantic Ocean. *Nature Geoscience* 9:523–528, https://doi.org/10.1038/NGEO2740.

Bosse, A., P. Testor, L. Houpert, P. Damien, L. Prieur, D. Hayes, V. Taillandier, X. Durrieu de Madron, F. D'Ortenzio, L. Coppola, and others. 2016. Scales and dynamics of submesoscale coherent vortices formed by deep convection in the northwestern Mediterranean Sea. *Journal of Geophysical Research* 121:7,716–7,742, https://doi.org/10.1002/2016JC012144.

Bromwich, D.H., A.B. Wilson, L.-S. Bai, G.W.K. Moore, and P. Bauer. 2016. A comparison of the regional Arctic System Reanalysis and the global ERA-Interim Reanalysis for the Arctic. *Quarterly Journal of the Royal Meteorological Society* 142:644–658, https://doi.org/10.1002/qj.2527.

Dee, D.P., S.M. Uppala, A.J. Simmons, P. Berrisford, P. Poli, S. Kobayashi, U. Andrae, M.A. Balmaseda, G. Balsamo, P. Bauer, and others. 2011. The ERA-Interim reanalysis: Configuration and performance of the data assimilation system. *Quarterly Journal of the Royal Meteorological Society* 137:553–597, https://doi.org/10.1002/qj.828.

de Jong, M.F., and L. de Steur. 2016. Strong winter cooling over the Irminger Sea in winter 2014–2015, exceptional deep convection, and the emergence of anomalously low SST. *Geophysical Research Letters* 43:7,106–7,113, https://doi.org/10.1002/2016GL069596.

de Jong, M.F., H.M. van Aken, K. Våge, and R.S. Pickart. 2012. Convective mixing in the central Irminger Sea: 2002–2010, *Deep Sea Research Part I* 63:36–51, https://doi.org/10.1016/j.dsr.2012.01.003.

Doyle, J.D., and M.A. Shapiro. 1999. Flow response to large-scale topography: The Greenland tip jet. *Tellus A* 51:728–748, https://doi.org/10.3402/tellusa.v51i5.14471.

Fan, X., U. Send, P. Testor, J. Karstensen, and P. Lherminier. 2013. Observations of Irminger Sea anticyclonic eddies. *Journal of Physical Oceanography* 43:805–823, https://doi.org/10.1175/JPO-D-11-0155.1.

Houpert, L., X. Durrieu de Madron, P. Testor, A. Bosse, F. D'Ortenzio, M.N. Bouin, D. Dausse, H. Le Goff, S. Kunesch, M. Labaste, and others. 2016. Observations of open-ocean deep convection in the northwestern Mediterranean Sea: Seasonal and interannual variability of mixing and deep water masses for the 2007–2013 period. *Journal of Geophysical Research* 121:8,139–8,171, https://doi.org/10.1002/2016JC011857.

Holdsworth, A.M., and P.G. Myers. 2015. The influence of high-frequency atmospheric forcing on the circulation and convection of the Labrador Sea. *Journal of Climate* 28:4,980–4,996, https://doi.org/10.1175/JCLI-D-14-00564.1.

Killworth, P.D. 1979. On chimney formation in the ocean. *Journal of Physical Oceanography* 9:531–554, https://doi.org/10.1175/1520-0485(1979)009<0531:OFITO>2.0.CO;2.

Lazier, J.R. 1973. The renewal of Labrador Sea Water. *Deep Sea Research* 20:341–353, https://doi.org/10.1016/0011-7471(73)90058-2.

Lozier, M., S. Bacon, A. Bower, S. Cunningham, M. de Jong, L. de Steur, B. deYoung, J. Fischer, S. Gary, B. Greenan, and others. 2017. Overturning in the Subpolar North Atlantic Program: A new international ocean observing system. *Bulletin of the American Meteorological Society* 98(4):737–752, https://doi.org/10.1175/BAMS-D-16-0057.1.

Marshall, J., and F. Schott. 1999. Open-ocean convection: Observations, theory and models. *Reviews of Geophysics* 37:1–64, https://doi.org/10.1029/98RG02739.

Moore, G.W.K. 2003. Gale force winds over the Irminger Sea to the east of Cape Farewell, Greenland. *Geophysical Research Letters* 30, 1894, https://doi.org/10.1029/2003GL018012.

Moore, G.W.K., D.H. Bronwich, A.B. Wilson, I. Renfrew, and L. Bai. 2016. Arctic system reanalysis improvements in topographically forced winds near Greenland. *Quarterly Journal of the Royal Meteorological Society* 142:2,033–2,045, https://doi.org/10.1002/qj.2798.

Moore, G.W.K., and I.A. Renfrew. 2005. Tip jets and barrier winds: A QuickSCAT climatology of high wind speed events around Greenland. *Journal of Climate* 18:3,713–3,725, https://doi.org/10.1175/JCLI3455.1.

Moore, G.W.K., I.A. Renfrew, B.E. Harden, and S.H. Mernild. 2015. The impact of resolution on the representation of southeast Greenland barrier winds and katabatic flows. *Geophysical Research Letters* 42:3,011–3,018, https://doi.org/10.1002/2015GL063550.

Nansen, F. 1912. Das Bodenwasser und die Abkuhlung des Meeres. *Internationale Revue der gesamten Hydrobiologie und Hydrographie* 5:1–42, https://doi.org/10.1002/iroh.19120050102.

Palevsky, H.I., and D.P. Nicholson. 2018. The North Atlantic biological pump: Insights from the Ocean Observatories Initiative Irminger Sea Array. *Oceanography* 31(1):42–49, https://doi.org/10.5670/oceanog.2018.108.

Pickart, R.S., F. Straneo, and G.W.K. Moore. 2003. Is Labrador Sea Water formed in the Irminger Basin? *Deep Sea Research Part I* 50(1):23–52, https://doi.org/10.1016/S0967-0637(02)00134-6.

Sverdrup, H.U., M.W. Johnson, and R.H. Fleming. 1942. *The Oceans: Their Physics, Chemistry, and General Biology*. Prentice-Hall Inc., Englewood Cliffs, NJ, USA, 1,060 pp.

Testor, A. Bosse, L. Houpert, F. Margirier, L. Mortier, H. Legoff, D. Dausse, M. Labaste, J. Karstensen, D. Hayes, and others. 2017. Multiscale observations of deep convection in the northwestern Mediterranean Sea during winter 2012–2013 using multiple platforms. *Journal of Geophysical Research*, https://doi.org/10.1002/2016JC012671.

Våge, K., R.S. Pickart, G.W.K. Moore, and M.H. Ribergaard. 2008. Winter mixed layer development in the central Irminger Sea: The effect of strong, intermittent wind events. *Journal of Physical Oceanography* 38:541–565, https://doi.org/10.1175/2007JPO3678.1.

Yashayaev, I., and J.W. Loder. 2017. Further intensification of deep convection in the Labrador Sea in 2016. *Geophysical Research Letters* 44:1,429–1,438, https://doi.org/10.1002/2016GL071668.

ACKNOWLEDGMENTS

The research leading to these results has received funding from the European Union's Horizon 2020 research and innovation program under grant agreement 633211 (AtlantOS) and grant agreement 727852 (Blue-Action), and from the European Union's Seventh Framework Program (FP7/2007-2013) under grant agreement 308299 (NACLIM) and grant agreement 312463 (FixO3). Data from the CIS and LOCO moorings are freely available from the OceanSITES database at http://www.oceansites.org. OOI data were obtained from the NSF Ocean Observatories Initiative Data Portal, http://ooinet.oceanobservatories.org, downloaded on August 9, 2017. We thank two anonymous reviewers as well as the guest editor, Tim Cowles, for suggestions that improved this manuscript.

AUTHORS

M. Femke de Jong (femke.de.jong@nioz.nl) is a tenure-track scientist at the Royal Netherlands Institute for Sea Research and Utrecht University, Texel, the Netherlands. **Marilena Oltmanns** is a research scientist and **Johannes Karstensen** is Senior Research Scientist, GEOMAR Helmholtz Centre for Ocean Research Kiel, Kiel, Germany. **Laura de Steur** is a research scientist at the Norwegian Polar Institute, Tromsø, Norway, and the Royal Netherlands Institute for Sea Research and Utrecht University, Texel, the Netherlands.

ARTICLE CITATION

de Jong, M.F., M. Oltmanns, J. Karstensen, and L. de Steur. 2018. Deep convection in the Irminger Sea observed with a dense mooring array. *Oceanography* 31(1):50–59, https://doi.org/10.5670/oceanog.2018.109.